Bottom up modeling of the connectome: linking structure and function in the resting brain and their changes in aging

Tristan T. Nakagawa, Viktor K. Jirsa, Andreas Spiegler, Anthony R. McIntosh, Gustavo Deco

PII: S1053-8119(13)00402-3
DOI: doi: 10.1016/j.neuroimage.2013.04.055
Reference: YNIMG 10367

To appear in: *NeuroImage*

Accepted date: 15 April 2013

Please cite this article as: Nakagawa, Tristan T., Jirsa, Viktor K., Spiegler, Andreas, McIntosh, Anthony R., Deco, Gustavo, Bottom up modeling of the connectome: linking structure and function in the resting brain and their changes in aging, *NeuroImage* (2013), doi: 10.1016/j.neuroimage.2013.04.055

Bottom up modeling of the connectome: linking structure and function in the resting brain and their changes in aging

Tristan T. Nakagawa[a,*], Viktor K. Jirsa[b], Andreas Spiegler[b], Anthony R. McIntosh[c], Gustavo Deco[a,d]

[a] *Center for Brain and Cognition, Computational Neuroscience Group, Department of Information and Communication Technologies, Universitat Pompeu Fabra, Barcelona, 08018, Spain*

[b] *Institut de Neurosciences des Systmes UMR INSERM 1106, Aix-Marseille Universit, 13005 Marseille, France*

[c] *Rotman Research Institute of Baycrest Centre, University of Toronto, Toronto, Ontario, Canada*

[d] *Instituci Catalana de la Recerca i Estudis Avanats, Universitat Pompeu Fabra, Barcelona, 08010, Spain*

Abstract

With the increasing availability of advanced imaging technologies, we are entering a new era of neuroscience. Detailed descriptions of the complex brain network enable us to map out a structural connectome, characterize it with graph theoretical methods, and compare it to the functional networks with increasing detail. To link these two aspects and understand how dynamics and structure interact to form functional brain networks in task and in the resting state, we use theoretical models. The advantage of using theoretical models is that by recreating functional connectivity and time series explicitly from structure and pre-defined dynamics, we can extract critical mechanisms by linking structure and function in ways not directly accessible in the real brain. Recently, resting state models with varying local dynamics have reproduced empirical functional connectivity patterns, and given support to the view that the brain works at a critical point at the edge of a bifurcation of the system. Here, we present an overview of a modeling approach of the resting brain network and give an application of a neural mass model in the study of complexity changes in aging.

Keywords: Structure-Function, Resting-State Models, criticality, MSE, Multiscale Entopy, Aging, Complexity

*Corresponding author, Email address: tristan.nakagawa@upf.edu
Email address: tristan.nakagawa@upf.edu (Tristan T. Nakagawa)

1. Introduction

With the turn of the millennium, a paradigm shift slowly occurred in the field of brain science. In the 1990s, driven by the maturation of fMRI and its high spatial resolution, studies mainly focused on the precise localization of specific brain functions, leading to a new level of understanding of many perceptual processing streams, the mapping of two visual pathways in the brain, and localization of various specific functions. However, with time it also became clear that many neural responses depend strongly on context. Also, complex brain functions such as attention and consciousness interact widely throughout the brain, and there are also networks of brain areas actively structuring brain dynamics in the absence of any task. Especially the latter sparked interest in the dynamics of the fixation-only or eyes-closed awake 'resting state' condition as a potential baseline for various task conditions, and the investigation of intrinsic structure, self-organizing principles and dynamics of the brain as a network of networks (Gusnard and Raichle, 2001). With concurring advances in DTI/DSI and related technologies it has been possible to create a first generation of structural macro-connectomes (Hagmann et al., 2008; Hagmann et al., 2010; Sporns et al., 2005; Sporns, 2011) as well as large-scale functionally connected networks in fMRI-BOLD (Damoiseaux et al., 2006; Doucet et al., 2011; Fox and Raichle, 2007; Fox et al., 2005; Greicius et al., 2003), and, most recently, MEG and EEG recordings (Brooks et al., 2011a; Brookes et al., 2011b; Hipp et al., 2012; Mantini et al., 2007; Yuan et al., 2012). Furthermore, we are now in the process of obtaining detailed structural and physiological descriptions of the brain on multiple scales at once for large, physiologically detailed reconstructions of its networks (Van Essen and Ugurbil, 2012; Van Essen et al., 2012).

However, a major challenge we will face in the coming years will not only be the pure recreation of realistic brain connectivity and dynamics. It will be the extraction of important features and mechanisms of these dynamics and of the network structure that are critical to brain function. This is critical to understand how this most complex network self-organizes into a very stable and consistent, yet flexible and adaptive system and its core components. In the following, we will review and discuss how large-scale theoretical brain models are crucial to bridging the gap between purely anatomical brain networks and their cognitive architectures by identifying key network properties underlying the empirically observable network dynamics. We will outline how modeling evidence supports the idea that the brain works in a critical region close to a bifurcation, and that these dynamics are common to resting-state models capturing the spatial patterns of spontaneous brain activity. Finally, we will apply this modeling approach to the study of Multiscale Entropy (MSE) in the aging brain, and give an outlook on how capturing spatiotemporal dynamics such as complexity and oscillatory dynamics presents the next big challenge for computational models, to contribute further to understanding cognitive architecture of the brain and its relation to the underlying structural connectome.

In following section, we will first describe how large scale computational models link the structural connectome to functional networks and dynamics.

We then exemplarily review the underlying architecture of a biophysically sophisticated resting-state model and its reduction to a neural mass model in section 3. Finally, in section 4, we give an application of the model for studying changes in cognitive architecture and complexity of spontaneous dynamics in aging.

2. Linking structure and dynamics: model approaches

An important question which remains to be answered in spite of the advances in structural mapping of the human connectome and intrinsic functional networks, is how they are related in detail. For large scale spontaneous fMRI dynamics, it has been shown that functional correlations of slow fluctuations are mainly determined by the underlying structural large-scale connectivity in the long run (Greicius et al, 2009; Hagmann et al., 2008; Honey et al., 2009; Skudlarski et al., 2008), and both functional and structural network characteristics can be described using graph theory (Bullmore and Bassett,2011; Sporns, 2011). However, this structure-function mapping is imperfect, as functional connectivities are also influenced by indirect links and network dynamics, especially on shorter time intervals (Honey et al., 2009). In this sense, the structural connectome is like a road system, in which traffic volume (functional connections) and street size are closely connected in the long run, but depend much more on the dynamics of the population on shorter time scales. Even though this analogy does not extend to the specific dynamics of the systems, it nicely illustrates the enabling (and limiting) role of structure for function. Analogously, our observations of functional relations and states may be strongly influenced by sampling window and frequency, as well as the aspects of the dynamics we focus on, such as mean activity, peak activity, or oscillatory phases.

As these dynamics enable the brain's rich repertoire of functional states, it is of fundamental theoretical interest to understand the critical features and mechanisms that link anatomical structure and recordings of brain dynamics. Theoretical models bridge this gap by constructing explicit network dynamics to capture the relations between structural connections and resulting resting-state recordings (Cabral et al., 2011; Deco and Jirsa, 2012; Deco et al., 2009; Deco et al., submitted for publication; Honey et al., 2007; Honey et al., 2009; Knock et al., 2009).

These models are all implemented on graphs with nodes (brain areas), edges (connections), and local node dynamics, as illustrated in Fig. (1). Spatial connectivity is determined by the parcellated structural connectome, derived from diffusion imaging (Hagmann et al., 2008) and tracing studies and databases (Gong et al., 2009; Ktter, 2004).

For modeling brain areas as nodes on the graph, raw diffusion data are parcelled, and areas and connectivities are down-sampled to the brain-area level and normalized. The resulting structural connectivity matrices are taken as fiber tracts between brain areas, and their functional transmission strength in the model is taken as the relative density of these tracts. The topological properties of the extracted brain network depend on, and are limited by the precision

of several parameters such as fiber extraction algorithms (see e.g. Hagman et al., 2008; methods section, for an exemplary analysis pipeline), extraction of connectivity direction, and cortex parcellation (Jbabdi et al., 2009; Wang et al, 2009; Zalesky et al., 2010). At least on low-resolution parcellations, though, our earlier work shows model robustness over different parcellations for exploration of large-scale BOLD patterns of structural and functional networks (Cabral et al., 2012).

Delays, reflecting finite transmission velocities along axonal fiber tracts, and which may reach up to 200ms in the human brain (Nuez, 1995) further shape the full spatiotemporal structure, especially in the presence of oscillatory local dynamics (Campbell, 2007; Freyer et al., 2011; Jirsa and Ding, 2004). Intrinsic local dynamics have been captured in models by simple (Cabral et al., 2011; Deco et al., 2009; Ghosh et al., 2008a; Ghosh et al., 2008b) and chaotic (Honey et al., 2007; Honey et al., 2009) oscillators as well as by detailed biophysically realistic descriptions of spiking neuron populations (Deco and Jirsa, 2012). Noise is added to keep the system active and in a dynamic regime in the absence of structured external input (Deco et al., 2009; Ghosh et al., 2008b).

The simulated time series for every node are then constructed as a forward model on the basis of local dynamics and input from other nodes arriving through the network structure. Functional connectivities are computed from the time series raw, phase or power correlations and related functional connectivity measures. Generally, for low couplings, the system nodes are in a state dominated by low activity (Deco and Jirsa, 2012; Ghosh et al., 2008b; Honey et al., 2007) or intrinsic oscillations (Deco et al., 2009, Cabral et al., 2011). With increasing coupling, the system transitions to higher activity or synchronization states, which are spatially structured by the topography of the underlying anatomical connectome. These structurals connections are important as they provide

As the global strength level of the connections is not known apriori, the optimal model working point can be determined by comparing the model and the empirical functional connectivities for different coupling strengths. For the different resting state models, this has commonly been found to be at the critical point of a bifurcation at the edge of instability; i.e. at the border between a stable homogenous baseline state and emergent activation or synchronization patterns (see Fig. 1,). Critical dynamics of fluctuations between unstable functional brain states have been suggested to occur in neural networks (Beggs, 2011; Haken, 1996, Rabinovich et al., 2001; Rabinovich et al., 2008), and there is ever increasing empirical and model evidence for criticality as an organizing principle in the brain as a whole (Basset et al., 2006; Kitzbichler et al., 2009; Poil et al., 2008; Poil et al., 2012; Tagliazucchi et al., 2012).

For global resting-state dynamics, the working location of the system at a critical point may maximize its flexibility and enable it to explore various functional states. Typical resting state dynamics with fluctuations between functional states occur as nodes transiently synchronize into sets of co-activated brain regions when being pushed beyond the bifurcation by noise. While the structure of the network depends on the underlying connectome, degree and

variability of expression for specific networks are shaped by the proximity to the bifurcation and the noise of the dynamics. From this perspective, the emergence of Resting-State Networks (RSN) reflect the dynamical capacity of the system to explore the brain's state space spontaneously while remaining able to efficiently respond to minimal external inputs. Recently, Deco and Jirsa (2012) have found such critical dynamics in a detailed and realistic spiking neuron attractor model, represented by populations of excitatory (AMPA and NMDA) and inhibitory (GABA-A receptor) integrate and fire neurons.

In the non-oscillatory, asynchrouneous state, as in the presented model, the key component to the model and its dynamics depend on the topography of its spatial connectivity structure and the location of its bifurcation, where the available states may change mainly with the graph properties of the network. In this case, the consistently reduced dynamic mean field model captures the resting state dynamics and bifurcation structure of the spiking model (Deco et al., submitted). This is not necessarily true in the presence of oscillations, as the delay structure and fast dynamics become important and must be taken into account as additional factors and the network interactions become more complex.

In the following, we will illustrate the bifurcation from a trivial low activity state to multistable attractors with this model, and how its reduction to a neural mass model can help us appreciate its main mechanisms and necessary preconditions.

3. Biophysical model characterization of the resting state

3.1. Spiking model

The spiking neuron model combines the large-scale network graph structure used in all full spatiotemporal resting state models with biophysically realistic populations of integrate-and-fire neurons on the microscopic scale. Fig. 1 shows the basic network setup.

In this model, each node is represented by an excitatory and an inhibitory population of leaky integrate-and-fire neurons with AMPA and NMDA, or GABA-A synaptic receptor types, respectively (Brunel and Wang, 2001). This type of network of spiking neuron network tends to settle in stationary states, so called attractors, typically characterized by a stable pattern of firing activity (Deco and Rolls, 2006; Deco et al., 2008), depending on its input level. External or even intrinsic noise that appears in the form of finite size effects can provoke destabilization of an attractor inducing therefore transitions between different stable attractors. The spiking activity of the local network is determined by the dynamics of the membrane potentials $V(t)$, which are governed by a set of equations relating $V(t)$ to leakage and synaptic activity I_{syn} (including a noise term). For the equations and parameter values, see the Appendix.

This model is very detailed, but due to the large number of equations computationally costly. In order to simplify the model and make simulations for different connectivity structures and multiple runs and parameters feasible, the

model can be reduced to a neural mass model under certain assumptions. Based on the mean field model of Brunel and Wang (2001), the dynamic mean field (Wong and Wang, 2006) simplifies the original spiking model by replacing the synaptic gating variables by a DC component and a Gaussian fluctuation term dependent only on external synaptic gating variables, reducing the latency of the dynamics to the slow NMDA component, and linearizing the input-output relation of the inhibitory inter-neurons and integrating them into the excitatory dynamical equation.

BOLD fMRI signal was simulated by means of the Balloon-Windkessel hemodynamic model of Friston et al. (2000,2003) and all parameters are taken from there. The model describes the perfusion changes based on neural activity (S_i in the reduced model) in each brain region causing a vasodilatatory signal with auto-regulatory feedback. The BOLD signal is then modeled as a static nonlinear function of volume and deoxyhemoglobin that comprises a volume-weighted sum of extra- and intra-vascular signals. In the context of the present simulations, the BOLD signal is vastly dominated by the linear contributions of the hemodynamic model and the nonlinearities do not impact the results.

While the model is restricted to modeling spontaneous low-rate activity below the stabilization of high-activity states due to the linearizations and reduction to slow dynamics, the reduced model captures both the bifurcation properties of the underlying spiking model and the empirical functional connectivity patterns at the critical working point (Fig. 1 e; Deco et al., submitted). This, and the closeness of the working point to the bifurcation, indicate that Resting State Dynamics do not fully explore the whole state-space of possible configurations available to the brain, but rather a lower-dimensional subspace of possible states consisting of "ghost" attractors, regions of state space at the edge of the bifurcation (Deco and Jirsa, 2012). In this perspective, RSN dynamics are equivalent to the brain wandering around in the atrium of our cognitive architecture. The criticality of the dynamics can be likened to the flexibility of movement within this architecture: below the working point, the system remains near the entrance and does not visit any functional states (no functional connectivity), whereas supercritical dynamics keep it located in specific sections. The situation at the critical point allows the system to move most freely, to efficiently access more specific building compartments (functional states) when prompted (by specific inputs). If this analogy holds true, explicit analysis of the model time course pattern dynamics and quantification with high-order moments such as variance or entropy can help us shed light on the detailed underlying computations at rest by making model performance comparable on more dimensions. The temporal dynamics between resting state patterns such as sequence orders of activation patterns or co-expression and responses to external stimulations or network damage should be evident also in the complexity and variability of the simulated time series, and provide empirically testable measures and predictions to understanding the brain's criticality.

In the following section, we will illustrate how dynamical biophysical markers such as complexity (described in detail in section 4.3) can provide an excellent comparison measure for model and empirical resting state dynamics. In this

ongoing work, we show first results relating empirical observations of decreasing spontaneous MSE in senescence to criticality and model dynamics, and demonstrate how dynamical markers provide quantifiable access to network dynamics beyond spatial pattern analysis.

4. Application: Modeling complexity in Aging

4.1. Brain structure changes in aging

Above, we have laid out how there is an important, yet complex relation between structural and functional brain connectivity, and that computational models find a certain regime of critical connectivity and network interactions optimize the dynamical properties and functional connectivities. This view implies that in the real brain, some mechanisms regulate effective brain connectivity to establish and maintain this regime. Fallacy of the system to do so should result in dysfunctional states. In line with this notion, brain connectivity is known or suspected to be altered in psychopathology (Bullmore and Sporns, 2009; Whitfield-Gabrieli and Ford, 2012). In fact, observable changes in brain connectivity Alstot et al., 2009; Honey and Sporns, 2008) and their functional consequences (Lynall et al., 2010; Supekar et al., 2008) allow us to further probe and improve our models, and, in turn, to better characterize neurological diseases and lesions (Cabral et al., 2012) in terms of their principle mechanisms. To better understand how changes in connectivity affect the brain dynamics, and to what extent the brain can adapt to those changes, we can use computational models.

This approach is not limited to the study of pathological states. Our brain network naturally changes over our lifespan, with maturation-related changes in childhood and both gray and white matter decreases in healthy, non-pathological aging. Many structural, cellular, and physiological mechanisms appear to tune our brain during its maturation to maximize its complexity and cognitive performance (Tononi et al., 1994; Lipp et al., 2009; McIntosh et al., 2008; Vakorin et al., 2011). In contrast, senescence is primarily associated with involuntary anatomical decline and decreasing complexity. Structural changes in adult aging have recently been mapped out in some detail with advances in high-resolution structural MR, DTI/DSI, tractography, and derived measures. Results still vary in the specifics, in part due to the still developing methodologies (Galluzi et al., 2008; Sullivan and Pfefferbaum, 2007; Giorgio et al., 2010; Gunning-Dixon et al, 2009). In general, though, both gray and white matter are found to decrease with age, with an anterior-posterior gradient in white matter (Ardekani et al., 2007; Grieve et al., 2007; Head et al., 2004; Pfefferbaum and Sullivan, 2003; Salat et al., 2005). Temporally, gray matter decreases approximately linear, while measurements of white matter changes are more heterogeneous: volume increases up to ages 30-40 and decreasing only from around age 50 in volume in most areas (Pfefferbaum, 1994; Ge et al., 2002; Giorgio et al., 2010), but diffusion measures show linear decay at this age already (Giorgio et al. 2010; Salat et al., 2005).

These changes in structure and structural connectivity with age are associated with decreases in cognitive performance: older adults show decreases in many aspects of cognition attributed to loss of processing speed (e.g. Salthouse, 1996), and aspects of executive functions including task switching and working memory seem especially vulnerable (Park et al., 2002). In trying to link cognitive decline with structural changes, some studies have found associations between gray matter volume and memory or cognitive performance in some areas (Salat et al., 2002; Rosen et al., 2003; Rodrigue and Raz, 2004, but see Tisserand et al., 2000; Gunning-Dixon and Raz, 2003 for contrary results). Decreases in white matter volume are related to executive function and memory (Brickman et al., 2006; Guttmann et al., 1998; Resnick et al., 2003), and micro-structural damage (white matter hyperintensities, WMH), have been linked to decreased processing speed and executive functions (DeCarli et al., 1995; Gunning-Dixon & Raz, 2000, 2003; Madden et al., 2009; Oosterman et al., 2004; Prins et al., 2005). Finally, processing speed and age have also been linked to lower brain signal complexity in recent studies (Garrett et al., 2011, 2012; McIntosh et al., 2008; McIntosh et al., 2010; McIntosh et al., submitted; Yang et al., 2012).

Here, we investigated how structural connectivity pruning (representing white matter losses) affects complexity in a large-scale computer model of resting state dynamics. To this end, we created connectomes with different levels of connectivity with two pruning algorithms (detailed in the methods section), and simulated resting state dynamics with a dynamic mean field model. We then calculated MSE from the time series, to test whether or not complexity can serve as a marker to distinguish different structural decline scenarios.

4.2. Model network structure

The global network structure determining the connectivity between the 74 nodes of the model was comprised of a combination of long-range and short-range connections. For the long-range connections, high resolution diffusion tensor images were down-sampled and parcellated into 74 areas to construct a coarse-grained connectivity matrix. These connections were extracted from a combination of diffusion spectrum MRI tractography and a mapping of the macaque connectome (CoCoMac database) onto the human brain (for details see Knock et al. (2009).

As DTI measures directionality of water diffusion in white matter tissue (Beaulieu et al., 2002), the more diffuse lateral connections along the cortical sheet are not detected by DTI measuring, and are here considered by short-range connectivity matrices.

These matrices used here were constructed from a Gaussian decaying connectivity on a triangulated cortical surface 'Cortex_reg13.mat' that is included in The Virtual Brain software package, available at http://thevirtualbrain.org/app/. The triangulated mesh that describes an individual cortical surface is based on a set of anatomical MRI scans. The mesh was obtained by extracting a high-resolution surface from MRI and sampling down the high-resolution surface, while balancing between curvature preservation and mesh regularity. The resulting surface composes the cortical geometry of 16,384 vertices and 32,760

triangles. Each vertex covers nearly 16 mm2 of the cortical sheet. Periodic boundaries conditioned the two hemispheres composed of 8,192 vertices each. To obtain the connectivity of each vertex with its neighborhood on the triangulated mesh, the edge lengths (with the mean of 3.9761 mm) were considered for sampling the short-range connectivity function (Spiegler and Jirsa, submitted). The short-range connectivity matrices used here differ in spatial decay of connectivity between vertices, with standard deviations of the gaussian spatial filter ranging between 10 mm and 40 mm. Each vertex of the cortical surface was then assigned to one of the 74 brain regions (37 per hemisphere), and the sum of the weighted lateral connections between vertices belonging to two different brain regions was taken as the short-range connectivity between those two regions.

To capture white-matter decreases, we studied the effects of long-range pruning by repeatedly decreasing the coupling weight of randomly selected node pairs of the long-range connectivities, and to capture decreasing lateral connections, we used short-range connectivity with increasingly faster spatial decay in steps of 10 mm. Matrices were combined in both cases, with pruning affecting selectively the short-range or the long-range contributions of the combined matrix. Simulations were run for four different connectivity levels, with a 16% connectivity decrease for every step, for both long-range pruning and short-range pruning.

To locate the system at Resting State dynamics, we here set the global coupling weight between nodes w to 3.50, where the original, unpruned matrix was at its critical point just below bifurcation. and simulations remained in an asynchronous low-firing regime.

4.3. Complexity and Multiscale Entropy

"Complexity" is a dynamic neurophysiological marker of efficient processing, cognitive performance and age, representing the richness of information in a system. For time series, it can be quantified by entropy-related measures such as MSE (Costa et al., 2002,2005) or Permutation Entropy (Richman and Moorman, 2000). Complexity has been linked to behavioral stability and task performance (McIntosh et al., 2008; McIntosh et al., 2010; Yang et al., 2012) as well as knowledge (Heisz et al., 2012). It increases in the early years of life (Lipp et al., 2009; McIntosh et al., 2008) as processing shifts from local to more distributed processing (Vakorin et al., 2011). This tuning process reflects the increasing functional differentiation with development. In older adults, less complex dynamics are observed at rest (Yang et al., 2012), and a smaller increase in complexity is observed in task (Garrett et al., 2012) or photic stimulation (Takahashi et al., 2009). These findings suggest that MSE can serve as a neurophysiological marker between underlying structure and functional network integrity or efficiency. Healthy, young brains are generally described by more complex time series, and Yang and colleagues' (2012) findings suggest that this relation can even be found in relatively short, resting fMRI data sets.

Many physiological systems produce irregular, complex time series, so highly regular states often mark dysfunction and disease (Pincus and Goldberger, 1994;

Goldberger et al., 2002). However, an increase in irregularity does not always mean an increase in complexity: noise signals are highly irregular and maximize entropy on the first temporal scale, but lose complexity quickly towards larger time scales (Goldberger et al., 2002): over longer periods, noise is deterministic, as it has one single expected mean value. To address this multiscale nature of truly complex time series, Costa et al. (2002, 2005) developed the MSE measure, which estimates sample entropy (Richman and Moorman, 2002) on the original time series as well as on down-sampled versions, revealing variability of the signal across different time scales. Given a time series x of length t, a down-sampled time series x_s is calculated for every scale factor s by constructing t/s non-overlapping windows of x, and taking the mean of all x in the window as new value for x_t, shortening x_s by the scale factor. Sample entropy is then calculated for each scale. It is defined as the negative natural logarithm of the conditional probability that sequences in a dataset that are similar for m data points (within similarity tolerance r, given as fraction of the standard deviation of the dataset) will remain similar adding another data point. We calculated MSE using the physionet (Goldberger et al., 2000) MSE algorithm (available at www.physionet.org/physiotools/mse/) both on the neuronal activity and the virtual BOLD signal for all simulations. For the BOLD signal, biophysical parameters were taken as in Friston et al. (2003), and sampling rate TR=2500ms and low-pass filtering (at .08 Hz) were set equal to the values in Yang et al. (2012) for comparability. To be able to calculate MSE for five time scales for the BOLD time series to and compare the results to empirical data, we used pattern length m=1 and similarity factor r=.35 (varied between .05 and .5 without changes in the results patterns). MSE was calculated from the neuronal time series at sampling resolution of 125 ms and from the BOLD signal at 2500 ms over scales 1:5 (2.5-12.5 s).

4.4. Complexity declines in aging

Results are presented from simulations of the dynamical mean field model for decreasing levels of structural connectivity, imitating the decreasing connectivity in the adult human brain. Network structure was derived from a combined anatomical connectome of long-range and short-range connections between brain areas, and the lower-connected matrices were constructed by pruning at one of the two ranges. For each pruning level and method, MSE was then calculated for both the neuronal time series and an fMRI BOLD model. For the rate model, both short-range and long-range pruning led to lower complexity values over all scales. As visible in Fig. 3, MSE decrease was strongest for the first pruning step. Entropy decreases with respect to the baseline were significant in all cases (all p-values $< .001$), resembling the difference between younger and older subjects in the empirical data, with no differences between short-range and long-range pruning (largest $t(18)$=1.60, $p = .13$).

MSE curves from the BOLD model time series are shown in Fig. 4. For all simulations using the BOLD model, there was an increase in entropy from scale 1 to 2, after which it gradually declined. This initial increase was not

visible in the empirical data of Yang et al.(2012), where the entropy values decreased gradually by about 0.1 from scales 1 to 5. The difference in the shape of the MSE curve appeared in spite of the fact that the same BOLD sampling, low-pass filtering, and MSE calculation parameters were used. On the second to fifth scales, the entropy values were quite similar in shape and amplitude to the empirical data, though with a steeper drop in complexity across scales. The increase in entropy in the model from the time scale of about 2.5 to 5-10 seconds indicates that the network dynamics are more regular on the fastest timescale, and that network interactions are therefore mainly shaped on the slower time scales. This is in line with the non-oscillatory network dynamics and slow NMDA component, producing slow BOLD fluctuations. The difference between model and empirical data on the fastest time scale may have various possible reasons,though. On the empirical side, scanner, movement or physiological artifacts may appear. Concerning neural dynamics, the model is in a low-firing regime producing slow BOLD fluctuations of several seconds (for detail, see Deco and Jirsa, 2012). At faster time scales, neural oscillations and local dynamics may modulate the dynamics of each node in a way that would not be captured by the model. However, if this were the case, the same pattern should be visible in rate-derived MSE measures. As the origin of this difference is unresolved and manifests on the fastest scale, we focus in the following on the slower time scales 3-5 (7.5-12.5s) for the BOLD signal. The effect of pruning was much smaller than for the neuronal rate (Fig. 5). There were no differences between the two pruning methods on any of the scales (largest $t(18) = .94$, $p = n.s.$), and the effect of decreasing the density of the connectome became apparent as an interaction of pruning and scales. The tendentially higher complexity of the pruned cases at the third scale (highest $t(9) = -2.67$, $p < .05$ for short range pruning; p-values for long-range pruning between .05 and .10, their difference n.s.) inverted to lower complexity at the slowest time scale ($t(9) = 3.14$, $p < .05$)) for all lower-connected cases (Fig. 4, top right panel). On this scale, the pruned case reached lower entropy values due to its steeper slope over lower scales (lowest $t(9) = -3.14$, $p < .05$). In summary, rate based measures showed concordance with empirical fMRI-BOLD MSE decreases with weakening connectivity. Model BOLD complexity showed lower entropy for lower connectivities on the largest scale only.

Here, we investigated the changes in dynamical complexity of a model of spontaneous large scale activity with decreasing connectivity. Connectome pruning was implemented by two different algorithms targeting diffuse lateral short-range connections along the cortical sheet and DTI-based white fiber tract long-range connections, respectively. MSE complexity measures were calculated from simulated neuronal and BOLD dynamics based on a large scale computational model of cortical resting state dynamics. From the model perspective, the decrease in complexity observed in the neuronal time series corresponded best to an increasing distance from the model working point at which the model best reproduces healthy resting state functional connectivity (Deco and Jirsa, 2012). This point lays just below the bifurcation from a global low activity state to the appearance of high firing states and multi-stability in the system. From

this point, as a consequence of pruning, mutual communication between the nodes becomes weaker and dynamics modulations from large-scale connectivity quickly decreased on large time scales.

The fact that the largest difference in entropy was caused by the first 16% of connectivity decline suggests that the resulting complexity of the model is most strongly affected near the dynamical working point of the model. Once the system is not near its dynamical working point anymore, the spontaneous dynamics of the nodes will be largely dominated by their internal dynamics. This may also be the reason why short-range and long-range pruning did not show differential effects on complexity: while the increasingly different connectomes may give rise to different network structures and attractor landscapes in high activity states, the main effect of connectivity reduction will be similar in the low-activity regime. In analogy, one would expect a similarly lower complexity in older brains due to structural decline and synaptic efficacy loss independent of the specific hypo-connection structure, while the form of the functional changes would depend on the specifics of the connectivity losses. For comparison, We show MSE curves for very high and low couplings in Inline Supplementary Figures 1 and 2. In line with our interpretation, MSE is highest for optimal coupling, and lower for both high and low-connected cases, with lowest MSE for low coupling strength. Note, however, that, the very high coupling state is not straightforward to interpret as it leaves the low activity regime for which the dynamic mean field is well defined.

The interpretation of these results is limited by the fact that, while pruning resulted in lower rate entropy over most scales as expected from the model, complexity of the simulated BOLD signal was affected much less clearly than expected. Here, the model did not reproduce the empirical pattern of steady decline and lower entropy for decreased connectivity occuring in old age over most scales. There may be various reasons for this. Surely, a network of similar nodes may only produce such effects that lay in the model dynamics and connectivity itself, and not those that may be due to changes in the local dynamics. This should, in principle, not only affect the BOLD dynamics differentially, but differences in sampling, filtering, and the BOLD conversion model itself introduce factors that may shape both signals differently.

In summary, both BOLD and rate signals did point towards lower complexity caused by structural connectivity decline on large scales. This effect may well be connected to the large proportion of cognitive performance decrease explained by processing speed changes in aging (Salthouse, 1996), as the system needs higher overall activation and provides lower communication efficiency. A more in depth comparison of pruning with and without compensatory shifting of the global or specific couplings, and pruning-related changes in graph properties are worthwhile topics for further investigation, e.g. in the context of stroke recovery.

4.5. Conclusions

So far, the major focus has been on the spatial components of resting state networks and their alteration due to external or internal factors. We are only

beginning to understand the spatiotemporal dynamics of RSN and their interactions. This is of particular interest to resting-state research, as complexity measures can be used as a biomarker of the network dynamics independent of external stimuli, and how the system is affected by different consciousness states and diseases. We suggest that scrutinizing complexity in models may contribute to a better understanding of the time scales of network interactions and allow for comparison of different models in terms of their ability to recreate observable complexity patterns across different scales.

We conclude that structural connectivity decrease led to lower complexity on slow time scales in a biophysically based computational large-scale model mainly in the rate dynamics. From the perspective of model, decreased MSE in older adults' resting fMRI time recordings can best be explained as a displacement of the system from its optimal dynamical working point. Multiscale complexity measures can be powerful tools to link the structural connectome to functional brain dynamics on various temporal scales and, as this study shows, can serve as functional biomarkers to link the dynamics and performance of virtual brain models to the richness of brain network activity.

4.6. Acknowledgements

The authors declare to have no conflicts of Interest. GD was supported by the ERC Advanced Grant: DYSTRUCTURE (n. 295129), by the Spanish Research Project SAF2010-16085 and by the CONSOLIDER-INGENIO 2010 Programme CSD2007-00012, and the FP7-ICT BrainScales. The research reported herein was supported by the Brain Network Recovery Group through the James S. McDonnell Foundation. TTN was supported by the SUR of the DEC of the Catalan Government and by the FSE. We thank Mohit Adhikari and Sven Hilbert for helpful comments on earlier versions of the manuscript.

5. Appendix A: Spiking model equations

In the following, the equations for the spiking and dynamic mean field are given. For the spiking model, each neuron's membrane voltage below threshold V_{thr} is governed by:

$$C_m \frac{dV(t)}{dt} = -g_m(V(t) - V_L) - I_{syn}(t), \tag{A.1}$$

with membrane capacitance C_m, leak conductance g_m, resting potential V_L and synaptic input current I_{syn}, where

$$I_{syn} = I_{AMPA,ext} + I_{AMPA,rec} + I_{NMDA} + I_{GABA} \tag{A.2}$$

,

$$I_{AMPA,ext}(t) = g_{AMPA,ext}(V(t) - V_E) \sum_{j=1}^{N_{ext}} s_j^{AMPA,ext}(t), \tag{A.3}$$

$$\frac{ds^{AMPA,ext}(t)}{dt} = \frac{s_j^{AMPA,ext}(t)}{\tau_{AMPA}} + \sum_k \delta(t - t_j^k), \tag{A.4}$$

$$I_{AMPA,rec}(t) = g_{AMPA,rec}(V(t) - V_E) \sum_{j=1}^{N_E} w_j s_j^{AMPA,rec}(t), \tag{A.5}$$

$$\frac{ds^{AMPA,rec}(t)}{dt} = \frac{s_j^{AMPA,rec}(t)}{\tau_{AMPA}} + \sum_k \delta(t - t_j^k), \tag{A.6}$$

$$I_{NMDA}(t) = \frac{g_{NMDA}(V(t) - V_E)}{1 + \lambda e^{-\beta V(t)}} \sum_{j=1}^{N_E} w_j s_j^{NMDA}(t), \tag{A.7}$$

$$\frac{ds^{NMDA}(t)}{dt} = -\frac{s_j^{NMDA}(t)}{\tau_{NMDA,decay}} + \alpha x_j(t)(1 - s_j^{NMDA}(t)), \tag{A.8}$$

$$\frac{dx^{NMDA}(t)}{dt} = \frac{x_j^{NMDA}(t)}{\tau_{NMDA,rise}} + \sum_k \delta(t - t_j^k), \tag{A.9}$$

$$I_{GABA}(t) = g_{GABA}(V(t) - V_I) \sum_{j=1}^{N_I} w_j s_j^{GABA}(t), \tag{A.10}$$

$$\frac{ds^{GABA}(t)}{dt} = \frac{s_j^{GABA}(t)}{\tau_{GABA}} + \sum_k \delta(t - t_j^k), \tag{A.11}$$

with synaptic conductances g, excitatory and inhibitory reversal potantials V_E and V_I, respectively, the Dirac-delta function δ, and synaptic weight parameter w_j (determining the connection strengths between and within neural populations). The gating variables s_j are the fractions of open ion channels of the neurons. Connections between excitatory and inhibitory pools were set to 1, and recurrent self-excitation to w+=1.5. Synaptic parameters were V_E=0mV, V_I=-70mV, τ_{AMPA}=2ms, $\tau_{NMDA,rise} = 2ms$, $\tau_{NMDA,decay} = 100ms$, τ_{GABA}=10ms, α=0.5kHz, β=0.062, γ=0.28. Once a neuron crosses V_{thr}, a spike is transmitted to connected neurons, and its membrane potential is reset to, and maintained at V_{reset} for refractory period τ_{ref}. All neurons in the network received an external background input from $N_{ext} = 800$ external AMPA signaling excitatory neurons injecting uncorrelated poisson-distributed spike trains, representing the noisy fluctuations that are typically observed *in vivo*. Specifically, for all neurons inside a given population p, the rate v_{ext}^p of the resulting global spike train is described by:

$$\tau_n \frac{dv_{ext}^p(t)}{dt} = -(v_{ext}^p(t) - v_0) + \sigma_v \sqrt[2]{2\tau_n} n^p(t), \tag{A.12}$$

where τ_n=300ms, v_0=2.4kHz, σ_v is the standard deviation of $v_{ext}^p(t)$, and $n^p(t)$ is normalized Gaussian white noise. Negative values of $v_{ext}^p(t)$ that could arise due to the noise term are rectified to zero.

After applying the mean field reduction to the above spiking model (Deco et al., submitted) , the activity is governed by:

$$\frac{dS_i(t)}{dt} = -\frac{S_i}{\tau_S} + (1 - S_i)\gamma H(x_i) + \sigma \upsilon_i(t), \tag{A.13}$$

$$H(x_i) = \frac{ax_i - b}{1 - exp(-d(ax_i - b))}, \tag{A.14}$$

$$x_i = wJ_N S_i + GJ_N \sum_j C_{ij} S_j + I_0, \tag{A.15}$$

where $H(x_i)$ and S_i denote the population rate and the average synaptic gating variable for each local cortical area, C_{ij} is the structural connectivity matrix containing the link strengths between brain areas i and j, and local excitatory recurrence is w(=0.9). Parameter values for the input output function are a=270 (VnC), b=108 (Hz), and d=0.154 (s). The kinetic parameters are γ=0.641/1000. (The factor 1000 is for expressing everything in ms), τ_S=100 (ms). The synaptic couplings are J_N=0.2609 (nA) and the overall effective external input is I_0=0.3 (nA). In equation (A.13), υ_i is uncorrelated standard Gaussian noise and the effective noise amplitude at each node is σ =0.001(nA).

6. References

References

[1] Alstott, J., Breakspear, M., Hagmann, P., Cammoun, L., Sporns, O., 2009. Modeling the impact of lesions in the human brain. PLoS Comput Biol 5, e1000408. URL: http://dx.doi.org/10.1371/journal.pcbi.1000408, doi:10.1371/journal.pcbi.1000408.

[2] Ardekani, S., Kumar, A., Bartzokis, G., Sinha, U., 2007. Exploratory voxel-based analysis of diffusion indices and hemispheric asymmetry in normal aging. Magn Reson Imaging 25, 154–167. URL: http://www.sciencedirect.com/science/article/pii/S0730725X06003365, doi:10.1016/j.mri.2006.09.045.

[3] Bassett, D.S., Meyer-Lindenberg, A., Achard, S., Duke, T., Bullmore, E., 2006. Adaptive reconfiguration of fractal small-world human brain functional networks. Proc Natl Acad Sci U S A 103, 19518–19523. doi:10.1073/pnas.0606005103. PMID: 17159150.

[4] Beaulieu, C., 2002. The basis of anisotropic water diffusion in the nervous system a technical review. NMR Biomed 15, 435455. URL: http://onlinelibrary.wiley.com/doi/10.1002/nbm.782/abstract, doi:10.1002/nbm.782.

[5] Beggs, J.M., 2008. The criticality hypothesis: how local cortical networks might optimize information processing. Philos Transact A Math Phys Eng Sci 366, 329–343. URL: http://www.ncbi.nlm.nih.gov/pubmed/17673410, doi:10.1098/rsta.2007.2092. PMID: 17673410.

[6] Brickman, A.M., Zimmerman, M.E., Paul, R.H., Grieve, S.M., Tate, D.F., Cohen, R.A., Williams, L.M., Clark, C.R., Gordon, E., 2006. Regional white matter and neuropsychological functioning across the adult lifespan. Biol Psychiatry 60, 444–453. doi:10.1016/j.biopsych.2006.01.011. PMID: 16616725.

[7] Brunel, N., Wang, X.J., 2001. Effects of neuromodulation in a cortical network model of object working memory dominated by recurrent inhibition. J Comput Neurosci 11, 6385.

[8] Bullmore, E., Sporns, O., 2009. Complex brain networks: graph theoretical analysis of structural and functional systems. Nat Rev Neurosci 10, 186–198. URL: http://dx.doi.org/10.1038/nrn2575, doi:10.1038/nrn2575.

[9] Bullmore, E.T., Bassett, D.S., 2011. Brain graphs: Graphical models of the human brain connectome. Annu Rev Clin Psychol 7, 113–140. URL: http://www.annualreviews.org/doi/abs/10.1146/annurev-clinpsy-040510-143934, doi:10.1146/annurev-clinpsy-040510-143934. PMID: 21128784.

[10] Cabral, J., Hugues, E., Kringelbach, M.L., Deco, G., 2012a. Modeling the outcome of structural disconnection on resting-state functional connectivity. NeuroImage 62, 1342–1353. URL: http://www.sciencedirect.com/science/article/pii/S1053811912005848, doi:10.1016/j.neuroimage.2012.06.007.

[11] Cabral, J., Hugues, E., Sporns, O., Deco, G., 2011. Role of local network oscillations in resting-state functional connectivity. Neuroimage URL: http://www.ncbi.nlm.nih.gov/pubmed/21511044, doi:10.1016/j.neuroimage.2011.04.010. PMID: 21511044.

[12] Cabral, J., Kringelbach, M., Deco, G., 2012b. Functional graph alterations in schizophrenia: A result from a global anatomic decoupling? Pharmacopsychiatry 45, S57–S64. URL: https://www.thieme-connect.com/DOI/DOI?10.1055/s-0032-1309001, doi:10.1055/s-0032-1309001.

[13] Campbell, S.A., 2007. Time delays in neural systems, in: McIntosh, A.R., Jirsa, V.K. (Eds.), Campbell, S.A., 2007. Time delays in neuHandbook of Brain Connectivity.. Springer-Verlag, Berlin, pp. 65–90.

[14] Costa, M., Goldberger, A.L., Peng, C.K., 2002. Multiscale entropy analysis of complex physiologic time series. Phys Rev Lett 89, 068102. URL: http://www.ncbi.nlm.nih.gov/pubmed/12190613. PMID: 12190613.

[15] Costa, M., Goldberger, A.L., Peng, C.K., 2005. Multiscale entropy analysis of biological signals. Phys Rev E Stat Nonlin Soft Matter Phys 71, 021906. URL: http://www.ncbi.nlm.nih.gov/pubmed/15783351. PMID: 15783351.

[16] Damoiseaux, J.S., Rombouts, S.A.R.B., Barkhof, F., Scheltens, P., Stam, C.J., Smith, S.M., Beckmann, C.F., 2006. Consistent resting-state networks across healthy subjects. Proc Natl Acad Sci U S A 103, 13848 – 13853. URL: http://www.pnas.org/content/103/37/13848.abstract, doi:10.1073/pnas.0601417103.

[17] DeCarli, C., Murphy, D.G., Tranh, M., Grady, C.L., Haxby, J.V., Gillette, J.A., Salerno, J.A., Gonzales-Aviles, A., Horwitz, B., Rapoport, S.I., 1995. The effect of white matter hyperintensity volume on brain structure, cognitive performance, and cerebral metabolism of glucose in 51 healthy adults. Neurology 45, 2077–2084. PMID: 7501162.

[18] Deco, G., Jirsa, V.K., 2012. Ongoing cortical activity at rest: Criticality, multistability, and ghost attractors. J Neurosci 32, 3366–3375. URL: http://www.jneurosci.org/content/32/10/3366, doi:10.1523/JNEUROSCI.2523-11.2012.

[19] Deco, G., Jirsa, V.K., McIntosh, A.R., Sporns, O., Ktter, R., 2009. Key role of coupling, delay, and noise in resting brain fluctuations. Proc Natl Acad Sci U S A 106, 10302.

[20] Deco, G., Jirsa, V.K., Robinson, P.A., Breakspear, M., Friston, K.J., 2008. The dynamic brain: From spiking neurons to neural masses and cortical fields. PLoS Comput Biol 4, e1000092.

[21] Deco, G., Ponce-Alvarez, A., Mantini, D., Romani, G.L., Hagmann, P., Corbetta, M., submitted for publication. Resting-state functional connectivity emerges from structurally and dynamically shaped slow linear fluctuations .

[22] Deco, G., Rolls, E.T., 2006. Decision-making and weber's law: a neurophysiological model. Eur J Neurosci 24, 901–916. doi:10.1111/j.1460-9568.2006.04940.x. PMID: 16930418.

[23] Deco, G., Senden, M., Jirsa, V., 2012. How anatomy shapes dynamics: a semi-analytical study of the brain at rest by a simple spin model. Front Comput Neurosci 6, 68. doi:10.3389/fncom.2012.00068. PMID: 23024632.

[24] Doucet, G., Naveau, M., Petit, L., Deicroix, N., {L. Zago}, Crivello, F., {Jobard, Gael}, {Tzourio-Mazoyer, Nathalie}, {Mazoyer, Bernard}, {Mellet, Emmanuel}, {Jollot, Marc}, 2011. Brain activity at rest: a multiscale hierarchical functional organization. J Neurophysiol .

[25] Fox, M.D., Raichle, M.E., 2007. Spontaneous fluctuations in brain activity observed with functional magnetic resonance imaging. Nat Rev Neurosci 8, 700–711. URL: http://dx.doi.org/10.1038/nrn2201, doi:10.1038/nrn2201.

[26] Fox, M.D., Snyder, A.Z., Vincent, J.L., Corbetta, M., Van Essen, D.C., Raichle, M.E., 2005. The human brain is intrinsically organized into dynamic, anticorrelated functional networks. Proc Natl Acad Sci U S A 102, 9673–9678. doi:10.1073/pnas.0504136102. PMID: 15976020 PMCID: 1157105.

[27] Freyer, F., Roberts, J.A., Becker, R., Robinson, P.A., Ritter, P., Breakspear, M., 2011. Biophysical mechanisms of multistability in resting-state cortical rhythms. J Neurosci 31, 6353–6361. URL: http://www.jneurosci.org/content/31/17/6353, doi:10.1523/JNEUROSCI.6693-10.2011.

[28] Friston, K.J., Harrison, L.M., Penny, W.D., 2003. Dynamic causal modelling. Neuroimage 19, 1273–1302. URL: http://www.sciencedirect.com/science/article/pii/S1053811903002027, doi:16/S1053-8119(03)00202-7.

[29] Friston, K.J., Mechelli, A., Turner, R., Price, C.J., 2000. Nonlinear responses in fMRI: the balloon model, volterra kernels, and other hemodynamics. Neuroimage 12, 466–477. doi:10.1006/nimg.2000.0630. PMID: 10988040.

[30] Galluzzi, S., Beltramello, A., Filippi, M., Frisoni, G.B., 2008. Aging. Neurol Sci 29, 296–300. URL: http://link.springer.com/article/10.1007/s10072-008-1002-6, doi:10.1007/s10072-008-1002-6.

[31] Garrett, D.D., Kovacevic, N., McIntosh, A.R., Grady, C.L., 2011. The importance of being variable. J Neurosci 31, 4496–4503. URL: http://www.ncbi.nlm.nih.gov/pmc/articles/PMC3104038/, doi:10.1523/JNEUROSCI.5641-10.2011. PMID: 21430150 PMCID: PMC3104038.

[32] Garrett, D.D., Kovacevic, N., McIntosh, A.R., Grady, C.L., 2012. The modulation of BOLD variability between cognitive states varies by age and processing speed. Cereb Cortex URL: http://cercor.oxfordjournals.org/content/early/2012/03/14/cercor.bhs055, doi:10.1093/cercor/bhs055.

[33] Ge, Y., Grossman, R.I., Babb, J.S., Rabin, M.L., Mannon, L.J., Kolson, D.L., 2002. Age-related total gray matter and white matter changes in normal adult brain. part i: volumetric MR imaging analysis. AJNR Am J Neuroradiol 23, 1327–1333. PMID: 12223373.

[34] Ghosh, A., Rho, Y., McIntosh, A.R., Ktter, R., Jirsa, V.K., 2008a. Cortical network dynamics with time delays reveals functional connectivity in the resting brain. Cogn Neurodyn 2, 115–120. doi:10.1007/s11571-008-9044-2. PMID: 19003478 PMCID: PMC2427063.

[35] Ghosh, A., Rho, Y.A., McIntosh, A.R., Ktter, R., Jirsa, V.K., 2008b. Noise during rest enables the exploration of the brain's dynamic repertoire. PLoS Comput Biol 4, e1000196. URL: http://dx.plos.org/10.1371/journal.pcbi.1000196, doi:10.1371/journal.pcbi.1000196.

[36] Giorgio, A., Santelli, L., Tomassini, V., Bosnell, R., Smith, S., De Stefano, N., Johansen-Berg, H., 2010. Age-related changes in grey and white matter structure throughout adulthood. Neuroimage 51, 943–951. URL: http://www.sciencedirect.com/science/article/pii/S1053811910002740, doi:10.1016/j.neuroimage.2010.03.004.

[37] Goldberger, A.L., Amaral, L.A.N., Glass, L., Hausdorff, J.M., Ivanov, P.C., Mark, R.G., Mietus, J.E., Moody, G.B., Peng, C.K., Stanley, H.E., 2000. PhysioBank, PhysioToolkit, and PhysioNet components of a new research resource for complex physiologic signals. Circulation 101, e215–e220. URL: http://circ.ahajournals.org/content/101/23/e215, doi:10.1161/01.CIR.101.23.e215.

[38] Goldberger, A.L., Peng, C.K., Lipsitz, L.A., 2002. What is physiologic complexity and how does it change with aging and disease? Neurobiol Aging 23, 23–26. URL: http://www.sciencedirect.com/science/article/pii/S0197458001002664, doi:10.1016/S0197-4580(01)00266-4.

[39] Gong, G., He, Y., Concha, L., Lebel, C., Gross, D.W., Evans, A.C., Beaulieu, C., 2009. Mapping anatomical connectivity patterns of human cerebral cortex using in vivo diffusion tensor imaging tractography. Cereb Cortex 19, 524–536. URL: http://cercor.oxfordjournals.org/content/19/3/524, doi:10.1093/cercor/bhn102.

[40] Greicius, M.D., Krasnow, B., Reiss, A.L., Menon, V., 2003. Functional connectivity in the resting brain: a network analysis of the default mode hypothesis. Proc Natl Acad Sci U S A 100, 253–258. URL: http://www.ncbi.nlm.nih.gov/pubmed/12506194, doi:10.1073/pnas.0135058100. PMID: 12506194.

[41] Greicius, M.D., Supekar, K., Menon, V., Dougherty, R.F., 2009. Resting-state functional connectivity reflects structural connectivity in the default mode network. Cereb Cortex 19, 72–78. URL: http://cercor.oxfordjournals.org/content/19/1/72, doi:10.1093/cercor/bhn059.

[42] Grieve, S.M., Williams, L.M., Paul, R.H., Clark, C.R., Gordon, E., 2007. Cognitive aging, executive function, and fractional anisotropy: A diffusion

tensor MR imaging study. AJNR Am J Neuroradiol 28, 226–235. URL: http://www.ajnr.org/content/28/2/226.

[43] Gunning-Dixon, F.M., Brickman, A.M., Cheng, J.C., Alexopoulos, G.S., 2009. Aging of cerebral white matter: a review of MRI findings. Int J Geriatr Psychiatry 24, 109–117. doi:10.1002/gps.2087. PMID: 18637641.

[44] Gunning-Dixon, F.M., Raz, N., 2000. The cognitive correlates of white matter abnormalities in normal aging: a quantitative review. Neuropsychology 14, 224–232. PMID: 10791862.

[45] Gunning-Dixon, F.M., Raz, N., 2003. Neuroanatomical correlates of selected executive functions in middle-aged and older adults: a prospective MRI study. Neuropsychologia 41, 1929–1941. PMID: 14572526.

[46] Gusnard, D.A., Raichle, M.E., 2001. Searching for a baseline: Functional imaging and the resting human brain. Nat Revies Neurosci 2, 685–694.

[47] Guttmann, C.R., Jolesz, F.A., Kikinis, R., Killiany, R.J., Moss, M.B., Sandor, T., Albert, M.S., 1998. White matter changes with normal aging. Neurology 50, 972–978. PMID: 9566381.

[48] Hagmann, P., Cammoun, L., Gigandet, X., Gerhard, S., Ellen Grant, P., Wedeen, V., Meuli, R., Thiran, J.P., Honey, C.J., Sporns, O., 2010. MR connectomics: Principles and challenges. J Neurosci Methods 194, 34–45. URL: http://www.sciencedirect.com/science/article/pii/S0165027010000361, doi:10.1016/j.jneumeth.2010.01.014.

[49] Hagmann, P., Cammoun, L., Gigandet, X., Meuli, R., Honey, C.J., Wedeen, V.J., Sporns, O., 2008. Mapping the structural core of human cerebral cortex. PLoS Biol 6, e159. URL: http://dx.doi.org/10.1371/journal.pbio.0060159, doi:10.1371/journal.pbio.0060159.

[50] Haken, H., 1996. Principles of brain functioning: a synergetic approach to brain activity, behavior, and cognition. Springer.

[51] Head, D., Buckner, R.L., Shimony, J.S., Williams, L.E., Akbudak, E., Conturo, T.E., McAvoy, M., Morris, J.C., Snyder, A.Z., 2004. Differential vulnerability of anterior white matter in nondemented aging with minimal acceleration in dementia of the alzheimer type: evidence from diffusion tensor imaging. Cereb Cortex 14, 410–423. PMID: 15028645.

[52] Heisz, J.J., Shedden, J.M., McIntosh, A.R., 2012. Relating brain signal variability to knowledge representation. Neuroimage 63, 1384–1392. URL: http://www.sciencedirect.com/science/article/pii/S1053811912008117, doi:10.1016/j.neuroimage.2012.08.018.

[53] Hipp, J.F., Hawellek, D.J., Corbetta, M., Siegel, M., Engel, A.K., 2012. Large-scale cortical correlation structure of spontaneous oscillatory activity. Nat Neurosci URL: http://www.nature.com/neuro/journal/vaop/ncurrent/full/nn.3101.html, doi:10.1038/nn.3101.

[54] Honey, C.J., Ktter, R., Breakspear, M., Sporns, O., 2007. Network structure of cerebral cortex shapes functional connectivity on multiple time scales. Proc Natl Acad Sci U S A 104, 10240 – 10245. URL: http://www.pnas.org/content/104/24/10240.abstract, doi:10.1073/pnas.0701519104.

[55] Honey, C.J., Sporns, O., Cammoun, L., Gigandet, X., Thiran, J.P., Meuli, R., Hagmann, P., 2009. Predicting human resting-state functional connectivity from structural connectivity. Proc Natl Acad Sci U S A 106, 2035 –2040. URL: http://www.pnas.org/content/106/6/2035.abstract, doi:10.1073/pnas.0811168106.

[56] Jbabdi, S., Woolrich, M.W., Behrens, T.E.J., 2009. Multiple-subjects connectivity-based parcellation using hierarchical dirichlet process mixture models. Neuroimage 44, 373–384. doi:10.1016/j.neuroimage.2008.08.044. PMID: 18845262.

[57] Jirsa, V.K., Ding, M., 2004. Will a large complex system with time delays be stable? Phys Rev Lett 93, 070602. URL: http://link.aps.org/doi/10.1103/PhysRevLett.93.070602, doi:10.1103/PhysRevLett.93.070602.

[58] Kitzbichler, M.G., Smith, M.L., Christensen, S.R., Bullmore, E., 2009. Broadband criticality of human brain network synchronization. PLoS Comput Biol 5. doi:10.1371/journal.pcbi.1000314. PMID: 19300473 PMCID: 2647739.

[59] Knock, S., McIntosh, A., Sporns, O., Ktter, R., Hagmann, P., Jirsa, V., 2009. The effects of physiologically plausible connectivity structure on local and global dynamics in large scale brain models. J Neurosci Methods 183, 86–94. URL: http://www.sciencedirect.com/science/article/pii/S0165027009003707, doi:10.1016/j.jneumeth.2009.07.007.

[60] Ktter, R., 2004. Online retrieval, processing, and visualization of primate connectivity data from the CoCoMac database. Neuroinformatics 2, 127–144. doi:10.1385/NI:2:2:127. PMID: 15319511.

[61] Lipp, S., Kovacevic, N., McIntosh, A.R., 2009. Differential maturation of brain signal complexity in the human auditory and visual system. Front Hum Neurosci 3. URL: http://www.ncbi.nlm.nih.gov/pmc/articles/PMC2783025/, doi:10.3389/neuro.09.048.2009. PMID: 19949455 PMCID: PMC2783025.

[62] Lynall, M.E., Bassett, D.S., Kerwin, R., McKenna, P.J., Kitzbichler, M., Muller, U., Bullmore, E., 2010. Functional connectivity and brain networks in schizophrenia. J Neurosci 30, 9477–9487. URL: http://www.jneurosci.org/content/30/28/9477, doi:10.1523/JNEUROSCI.0333-10.2010.

[63] Madden, D.J., Bennett, I.J., Song, A.W., 2009. Cerebral white matter integrity and cognitive aging: Contributions from diffusion tensor imaging. Neuropsychol Rev 19, 415–435. URL: http://www.ncbi.nlm.nih.gov/pmc/articles/PMC2787975/, doi:10.1007/s11065-009-9113-2. PMID: 19705281 PMCID: PMC2787975.

[64] Mantini, D., Perrucci, M.G., Del Gratta, C., Romani, G.L., Corbetta, M., 2007. Electrophysiological signatures of resting state networks in the human brain. Proc Natl Acad Sci U S A 104, 13170 – 13175. URL: http://www.pnas.org/content/104/32/13170.abstract, doi:10.1073/pnas.0700668104.

[65] McIntosh, A.R., Kovacevic, N., Itier, R.J., 2008. Increased brain signal variability accompanies lower behavioral variability in development. PLoS Comput Biol 4, e1000106. URL: http://dx.plos.org/10.1371/journal.pcbi.1000106, doi:10.1371/journal.pcbi.1000106.

[66] McIntosh, A.R., Kovacevic, N., Lippe, S., Garrett, D., Grady, C., Jirsa, V., 2010. The development of a noisy brain. Arch Ital Biol 148, 323–337. URL: http://www.architalbiol.org/aib/article/view/148323, doi:10.4449/aib.v148i3.1225.

[67] McIntosh, A.R., Vakorin, V.A., Kovacevic, N., Wang, H.Y., Diaconescu, A., Protzner, A., submitted for publication. Spatiotemporal dependency of age-related changes in brain signal variability .

[68] Nunez, P.L., 1995. Neocortical Dynamics and Human EEG Rhythms. 1st ed., Oxford University Press, USA.

[69] Oosterman, J.M., Sergeant, J.A., Weinstein, H.C., Scherder, E.J.A., 2004. Timed executive functions and white matter in aging with and without cardiovascular risk factors. Rev Neurosci 15, 439–462. PMID: 15656288.

[70] Park, D.C., Lautenschlager, G., Hedden, T., Davidson, N.S., Smith, A.D., Smith, P.K., 2002. Models of visuospatial and verbal memory across the adult life span. Psychol Aging 17, 299–320. doi:10.1037/0882-7974.17.2.299.

[71] Pfefferbaum, A., Sullivan, E.V., 2003. Increased brain white matter diffusivity in normal adult aging: relationship to anisotropy and partial voluming. Magn Reson Med 49, 953–961. doi:10.1002/mrm.10452. PMID: 12704779.

[72] Pfefferbaum A, M.D., 1994. A quantitative magnetic resonance imaging study of changes in brain morphology from infancy to late adulthood. Arch Neurol 51, 874–887. URL: http://dx.doi.org/10.1001/archneur.1994.00540210046012, doi:10.1001/archneur.1994.00540210046012.

[73] Pincus, S.M., Goldberger, A.L., 1994. Physiological time-series analysis: what does regularity quantify? Am J Physiol 266, H1643–1656. PMID: 8184944.

[74] Poil, S.S., Hardstone, R., Mansvelder, H.D., Linkenkaer-Hansen, K., 2012. Critical-state dynamics of avalanches and oscillations jointly emerge from balanced excitation/inhibition in neuronal networks. J Neurosci 32, 9817–9823. doi:10.1523/JNEUROSCI.5990-11.2012. PMID: 22815496.

[75] Poil, S.S., van Ooyen, A., Linkenkaer-Hansen, K., 2008. Avalanche dynamics of human brain oscillations: Relation to critical branching processes and temporal correlations. Hum Brain Mapp 29, 770777. URL: http://onlinelibrary.wiley.com/doi/10.1002/hbm.20590/abstract, doi:10.1002/hbm.20590.

[76] Prins, N.D., van Dijk, E.J., den Heijer, T., Vermeer, S.E., Jolles, J., Koudstaal, P.J., Hofman, A., Breteler, M.M.B., 2005. Cerebral small-vessel disease and decline in information processing speed, executive function and memory. Brain 128, 2034–2041. doi:10.1093/brain/awh553. PMID: 15947059.

[77] Rabinovich, M., Volkovskii, A., Lecanda, P., Huerta, R., Abarbanel, H.D., Laurent, G., 2001. Dynamical encoding by networks of competing neuron groups: winnerless competition. Phys Rev Lett 87, 068102. PMID: 11497865.

[78] Rabinovich, M.I., Huerta, R., Varona, P., Afraimovich, V.S., 2008. Transient cognitive dynamics, metastability, and decision making. PLoS Comput Biol 4, e1000072. doi:10.1371/journal.pcbi.1000072. PMID: 18452000.

[79] Resnick, S.M., Pham, D.L., Kraut, M.A., Zonderman, A.B., Davatzikos, C., 2003. Longitudinal magnetic resonance imaging studies of older adults: A shrinking brain. J Neurosci 23, 3295–3301. URL: http://www.jneurosci.org/content/23/8/3295.

[80] Richman, J.S., Moorman, J.R., 2000. Physiological time-series analysis using approximate entropy and sample entropy. Am J Physiol Heart Circ Physiol 278, H2039–H2049. URL: http://ajpheart.physiology.org/content/278/6/H2039.

[81] Rodrigue, K.M., Raz, N., 2004. Shrinkage of the entorhinal cortex over five years predicts memory performance in healthy adults. J Neurosci 24, 956–963. doi:10.1523/JNEUROSCI.4166-03.2004. PMID: 14749440.

[82] Rosen, A.C., Prull, M.W., Gabrieli, J.D.E., Stoub, T., O'Hara, R., Friedman, L., Yesavage, J.A., deToledo-Morrell, L., 2003. Differential associations between entorhinal and hippocampal volumes and memory performance in older adults. Behav Neurosci 117, 1150–1160. doi:10.1037/0735-7044.117.6.1150. PMID: 14674836.

[83] Salat, D., Tuch, D., Greve, D., van der Kouwe, A., Hevelone, N., Zaleta, A., Rosen, B., Fischl, B., Corkin, S., Rosas, H.D., Dale, A., 2005. Age-related alterations in white matter microstructure measured by diffusion tensor imaging. Neurobiol Aging 26, 1215–1227. URL: http://www.sciencedirect.com/science/article/pii/S0197458004003173, doi:10.1016/j.neurobiolaging.2004.09.017.

[84] Salat, D.H., Kaye, J.A., Janowsky, J.S., 2002. Greater orbital prefrontal volume selectively predicts worse working memory performance in older adults. Cereb Cortex 12, 494–505. PMID: 11950767.

[85] Salthouse, T.A., 1996. The processing-speed theory of adult age differences in cognition. Psychol Rev 103, 403–428. doi:10.1037/0033-295X.103.3.403.

[86] Senden, M., Goebel, R., Deco, G., 2012. Structural connectivity allows for multi-threading during rest: The structure of the cortex leads to efficient alternation between resting state exploratory behavior and default mode processing. Neuroimage 60, 2274–2284. URL: http://www.sciencedirect.com/science/article/pii/S105381191200239X, doi:10.1016/j.neuroimage.2012.02.061.

[87] Skudlarski, P., Jagannathan, K., Calhoun, V.D., Hampson, M., Skudlarska, B.A., Pearlson, G., 2008. Measuring brain connectivity: diffusion tensor imaging validates resting state temporal correlations. Neuroimage 43, 554–561. URL: http://www.ncbi.nlm.nih.gov/pubmed/18771736, doi:10.1016/j.neuroimage.2008.07.063. PMID: 18771736.

[88] Spiegler, A., Jirsa, V.K., submitted for publication. Systematic approximations of neural fields through 1 networks of neural masses in the virtual brain .

[89] Sporns, O., 2011. The human connectome: a complex network. Ann N Y Acad Sci 1224, 109–125. URL: http://sauwok5.fecyt.es/apps/full_record.do?product=UA&search_mode=GeneralSearch&qid=1&SID=S16AeIdJpF@6fclHoJk&page=1&doc=6, doi:10.1111/j.1749-6632.2010.05888.x.

[90] Sullivan, E.V., Pfefferbaum, A., 2007. Neuroradiological characterization of normal adult ageing. Brit J Radiol 80, S99–S108. doi:10.1259/bjr/22893432.

[91] Supekar, K., Menon, V., Rubin, D., Musen, M., Greicius, M.D., 2008. Network analysis of intrinsic functional brain connectivity in alzheimer's disease. PLoS Comput Biol 4. URL: http://www.ncbi.nlm.nih.gov/pmc/articles/PMC2435273/, doi:10.1371/journal.pcbi.1000100. PMID: 18584043 PMCID: PMC2435273.

[92] Tagliazucchi, E., Balenzuela, P., Fraiman, D., Chialvo, D.R., 2012. Criticality in large-scale brain FMRI dynamics unveiled by a novel point process analysis. Front Physiol 3, 15. doi:10.3389/fphys.2012.00015. PMID: 22347863.

[93] Takahashi, T., Cho, R.Y., Murata, T., Mizuno, T., Kikuchi, M., Mizukami, K., Kosaka, H., Takahashi, K., Wada, Y., 2009. Age-related variation in EEG complexity to photic stimulation: a multiscale entropy analysis. Clin Neurophysiol 120, 476–483. doi:10.1016/j.clinph.2008.12.043. PMID: 19231279.

[94] Tisserand, D.J., Visser, P.J., van Boxtel, M.P., Jolles, J., 2000. The relation between global and limbic brain volumes on MRI and cognitive performance in healthy individuals across the age range. Neurobiol Aging 21, 569–576. PMID: 10924774.

[95] Tononi, G., Sporns, O., Edelman, G.M., 1994. A measure for brain complexity: relating functional segregation and integration in the nervous system. Proc Natl Acad Sci U S A 91, 5033–5037. URL: http://www.pnas.org/content/91/11/5033.

[96] Vakorin, V.A., Lipp, S., McIntosh, A.R., 2011. Variability of brain signals processed locally transforms into higher connectivity with brain development. J Neurosci 31, 6405–6413. URL: http://www.jneurosci.org/content/31/17/6405, doi:10.1523/JNEUROSCI.3153-10.2011.

[97] Van Essen, D., Ugurbil, K., 2012. The future of the human connectome. Neuroimage 62, 1299–1310. URL: http://www.sciencedirect.com/science/article/pii/S1053811912000493, doi:10.1016/j.neuroimage.2012.01.032.

[98] Van Essen, D., Ugurbil, K., Auerbach, E., Barch, D., Behrens, T., Bucholz, R., Chang, A., Chen, L., Corbetta, M., Curtiss, S., Della Penna, S., Feinberg, D., Glasser, M., Harel, N., Heath, A., Larson-Prior, L., Marcus, D., Michalareas, G., Moeller, S., Oostenveld, R., Petersen, S., Prior, F., Schlaggar, B., Smith, S., Snyder, A., Xu, J., Yacoub, E., 2012. The human connectome project: A data acquisition perspective. Neuroimage 62, 2222–2231. URL: http://www.sciencedirect.com/science/article/pii/S1053811912001954, doi:10.1016/j.neuroimage.2012.02.018.

[99] Wang, J., Wang, L., Zang, Y., Yang, H., Tang, H., Gong, Q., Chen, Z., Zhu, C., He, Y., 2009. Parcellation-dependent small-world brain functional networks: A resting-state fMRI study Hum Brain Mapp 30, 15111523. URL: http://onlinelibrary.wiley.com/doi/10.1002/hbm.20623/abstract, doi:10.1002/hbm.20623.

[100] Whitfield-Gabrieli, S., Ford, J.M., 2012. Default mode network activity and connectivity in psychopathology. Annu Rev Clin Psychol 8, 49–76. URL: http://www.annualreviews.org/doi/

abs/10.1146/annurev-clinpsy-032511-143049, doi:10.1146/annurev-clinpsy-032511-143049. PMID: 22224834.

[101] Wong, K.F., Wang, X.J., 2006. A recurrent network mechanism of time integration in perceptual decisions. J Neurosci 26, 1314–1328. URL: http://www.jneurosci.org/cgi/content/abstract/26/4/1314, doi:10.1523/JNEUROSCI.3733-05.2006.

[102] Yang, A.C., Huang, C.C., Yeh, H.L., Liu, M.E., Hong, C.J., Tu, P.C., Chen, J.F., Huang, N.E., Peng, C.K., Lin, C.P., Tsai, S.J., 2012. Complexity of spontaneous BOLD activity in default mode network is correlated with cognitive function in normal male elderly: a multiscale entropy analysis. Neurobiol Aging URL: http://www.sciencedirect.com/science/article/pii/S019745801200276X, doi:10.1016/j.neurobiolaging.2012.05.004.

[103] Yuan, H., Zotev, V., Phillips, R., Drevets, W.C., Bodurka, J., 2012. Spatiotemporal dynamics of the brain at rest exploring EEG microstates as electrophysiological signatures of BOLD resting state networks. Neuroimage 60, 2062–2072. URL: http://www.sciencedirect.com/science/article/pii/S105381191200208X, doi:10.1016/j.neuroimage.2012.02.031.

[104] Zalesky, A., Fornito, A., Harding, I.H., Cocchi, L., Ycel, M., Pantelis, C., Bullmore, E.T., 2010. Whole-brain anatomical networks: Does the choice of nodes matter? NeuroImage 50, 970–983. URL: http://www.sciencedirect.com/science/article/pii/S1053811909013159, doi:10.1016/j.neuroimage.2009.12.027.

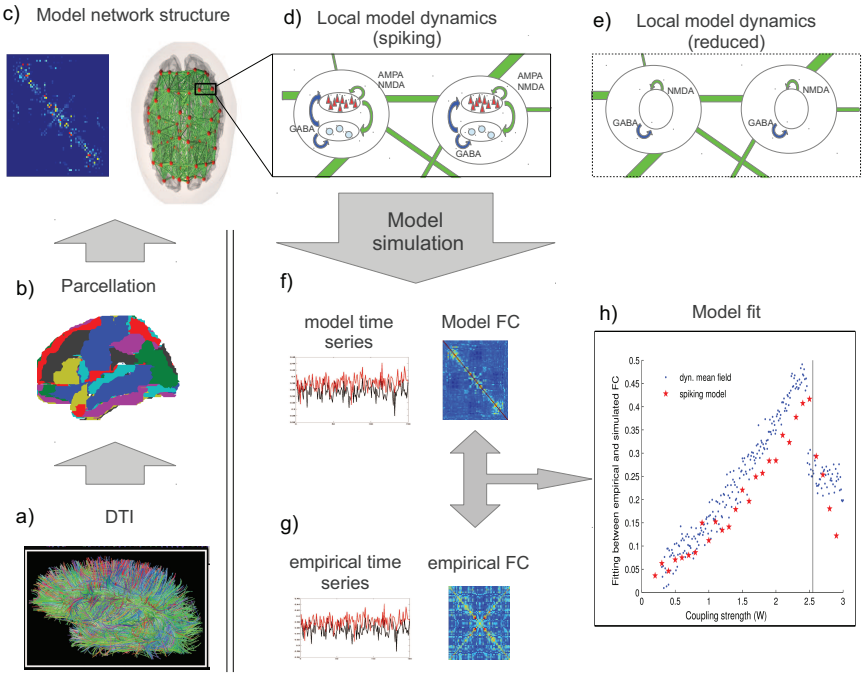

Figure 1: Modeling resting state networks. a) Fiber tract measurements (here depicting DTI, adopted and modified under a creative commons attribution licence, from Hagmann et al. (2007), b) parcellated from voxel space to brain areas, are used to build a brain graph (c, right), with nodes (red) representing brain areas and edges (green) represent edges between nodes.The coupling matrix (c, left), determining the relative weights of connections between nodes, allows the network nodes to interact with each other, depending on their local dynamics. Local model dynamics are exemplarily sketched out for the full spiking model (d) and its dynamic mean field reduction (e) as described in section 3. Functional connectivity from simulations (f) and empirical resting-state recordings (g) can then be compared to find the models working point, as depicted in (f) for the described model (adapted with permission from the authors, from Deco et al., submitted). The vertical black line shows the location of the bifurcation at wh the spontaneous stable state loses its stability.

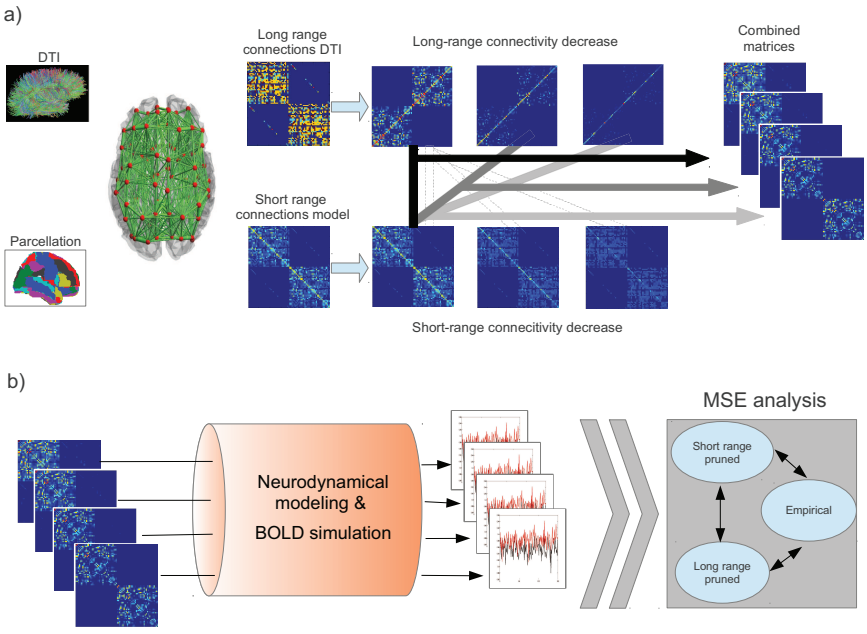

Figure 2: Methods: a) Construction of matrices representing connectivity decreases found in aging. A brain graph (second to left) is constructed from DTI fibre estimations between brain areas. Each node on the graph (red) represents a brain area, and connection strengths (green) determine the values in the connectivity matrices. To determine if there are differential effects, short-range and long-range connections are pruned separately, and matrices are then combined (shown for long-range pruning). b) Simulation and analysis pipeline. Dynamic mean field simulations are run for different levels of connectivity decrease for both scenarios, and BOLD time series are simulated for complexity (MSE) analysis.

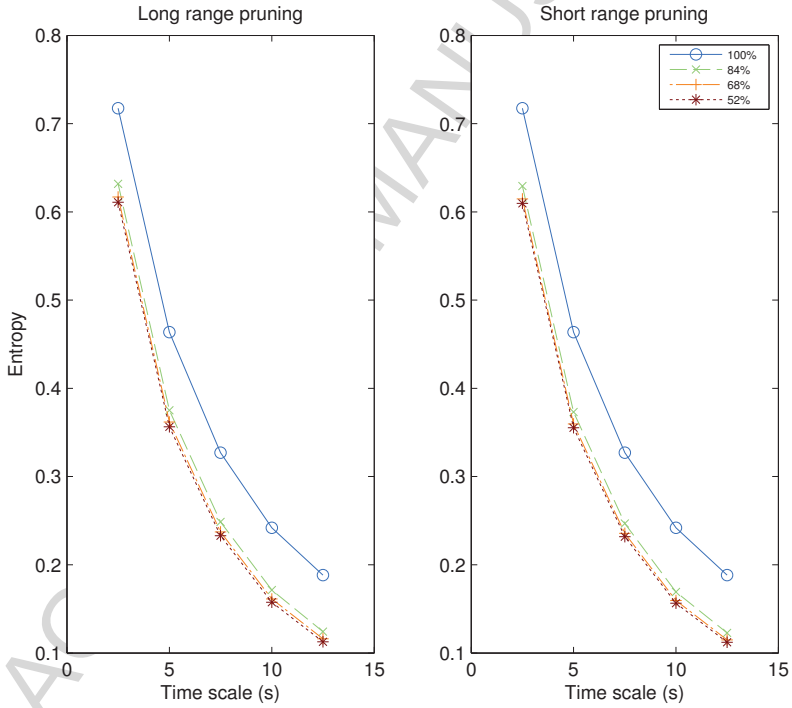

Figure 3: Rate MSE: MSE curves calculated from the down-sampled time series of the dynamic mean field model for time scales from 2.5s to 12.5s.

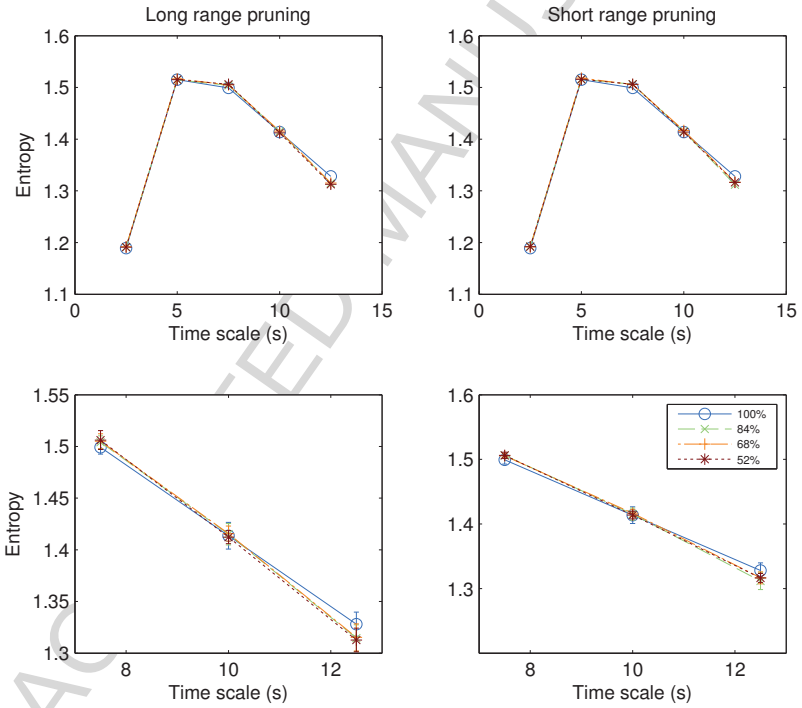

Figure 4: BOLD MSE: MSE curves calculated from the simulated BOLD time series of the model. Top row: BOLD scales 2.5s-12.5s, bottom row: closeup of top row at the slowest scales. Error bars in lower panels depict standard deviations.

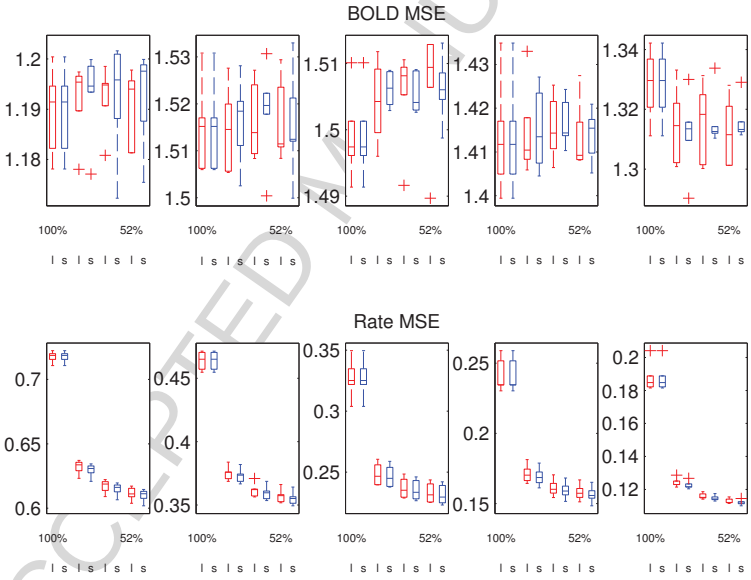

Figure 5: MSE Boxplots: Boxplots of MSE values from ten trials for all scales, for BOLD (top row) and for rate (bottom row) MSE. Each panel shows one boxplot for each connectivity density (100%, 84%, 68%, 52%) for long-range pruning (red, 'l') and short-range pruning (blue, 's'). Boxplots are centered on the median and are limited by the quartiles, and whiskers extend by a factor of 1.5. Outliers are marked by '+'.

Highlights

Manuscript title: “Bottom up modeling of the connectome: linking structure and function in the resting brain and their changes in aging”
Authors: Tristan T. Nakagawa, Viktor K. Jirsa, Andreas Spiegler, Anthony R. McIntosh, Gustavo Deco

Highlights

- Theoretical models link structural connectivity to brain dynamics
- Resting-state models successfully capture neural spatiotemporal patterns
- Criticality enables flexibility between network states and dynamics
- Models can be used to study dynamical markers (e.g. complexity) in disease and aging